An efficient FE analysis for complex low flying air bearing slider designs in hard disk drives: Part I Static Solution

Puneet Bhargava and David B. Bogy

Computer Mechanics Laboratory

Department of Mechanical Engineering

University of California at Berkeley

Berkeley, CA 94720

Telephone: (510) 642-4975

Fax: (510) 643-9786

puneet@cml.me.berkeley.edu

April 13, 2008

Abstract

Prediction of the steady state flying height and attitude of air bearing sliders in hard disk drives via simulations is the basis of their design process. Over the past few years air bearing surfaces have become increasingly complex incorporating deep etches and steep wall profiles. In this paper we present a novel method of solving the inverse problem for air-bearing sliders in hard disk drives that works well for such new designs. We also present a new method for calculating the static air-bearing stiffness by solving three linear systems. The formulation is implemented and convergence studies are carried out for the method. Mesh refinements based on flux jumps and pressure gradients are found to work better than those based on other criteria.

1 Introduction

The hard disk drive industry continually faces a demand for higher data areal densities and access speeds. This in turn translates into a need for lower fly heights for the read/write heads. The lower fly heights and the demand for increased reliability requires extremely complex slider geometries with steep etches that define the air bearing surface shapes. In order to evaluate such designs, there is a need for fast, reliable simulations of their flying characteristics. Thus there is a need for a simulation program that can solve for the flying height and attitude of complicated slider designs as quickly as possible.

The most important criteria in evaluating the design of an air bearing slider is the attitude of the slider in the steady state and the stiffness of the air bearing. The solution of the steady state problem is also often used as an initial condition to many dynamic problems such as shock and slider unloading. Hence the solution to the steady state problem is important. It can be obtained by directly solving a time-independent system. The alternative of performing a transient analysis until steady state is reached is much more expensive.

1

2   Previous Work

The problem of obtaining the static flying height and attitude of hard disk drive air-bearing sliders has previously been solved by various researchers in academia and industry. An excellent survey of these works was presented by Holani and Müftü (2005). These studies have used various approaches, such as the finite difference (White and Nigam, 1980; Castelli and Pirvics, 1968), finite volume (Hu and Bogy, 1995; Wu and Bogy, 2000; Cha and Bogy, 1995) and finite element (Smith, Wahl, and Talke, 1995; Garcia-Suarez, Bogy, and Talke, 1984; Hendricks, 1988; Kubo, Ohtsubo, Kawashima, and Marumo, 1988; Peng and Hardie, 1995) methods for solving this problem. The equilibrium attitude of the slider depends on the suspension forces and the air pressure acting on the slider. Various methods have been proposed to accomplish the coupling between the two sets of equations (structural and air-bearing). One approach includes the dynamic effects of the air bearing (i.e. the squeeze term for the Reynolds equation and inertial effects for the slider) (Tang, 1972; Ono, 1972; White and Nigam, 1980; Miu and Bogy, 1986; Ruiz and Bogy, 1990; Cha and Bogy, 1995). The steady state flying attitude is found by computing the transient solution until a steady state condition has been achieved. Another completely different approach obtains the coupled solution by formulating the problem for the steady state by neglecting the time-dependent terms (Yamaura and Ono, 1990; Choi and Yoon, 1994; Smith et al., 1995). As stated by Holani and Müftü (2005), probably the most challenging problem with numerical methods is the need to discretize a continuous domain into one with finite discrete parameters. The finite difference method typically requires a structured mesh and is thus limited in its mesh refinement capabilities. Wu and Bogy (2000) presented a finite volume method with unstructured triangular meshing to solve the Generalized Reynolds Equation. Also, finite element methods do not require a structured mesh. This offers a major advantage in that it renders the method highly suitable for local adaptive mesh refinement

using geometry and pressure gradients.

In this paper we present a new formulation for dealing with the *inverse problem* wherein the nonlinear structural-fluid coupling is linearized along with the Reynolds equation to solve just one set of iterations, instead of two (solving for the slider attitude in one, and solving the nonlinear Reynolds equation in the other). We also present a new method of obtaining air bearing stiffness wherein the exact stiffness matrix is obtained by solving a set of 3 linear problems, as opposed to the conventional perturbation method where three nonlinear systems are required to solve for the directional stiffness and 6 nonlinear systems are needed to solve for centered stiffness matrices. We also present a new hybrid strategy for mesh refinement that uses pressure gradient and flux jumps across elements to give rapid spatial grid convergence.

3   Methodology

When the slider (assumed to be rigid) flies on the disk, it's motion is governed by the following equation:

$$\mathbf{M}\,\ddot{\mathbf{x}} + \mathbf{C}\,\dot{\mathbf{x}} + \mathbf{K}\,\mathbf{x} + \mathbf{F}_{susp} = \mathbf{F}_{abs}(\mathbf{x}, \dot{\mathbf{x}}) + \mathbf{F}_{con}(\mathbf{x}) \tag{1}$$

where $\mathbf{x}$ is the vector of the 6 degrees of freedom of the slider, namely displacements and rotations in the x, y and z directions (see Fig. 1). To calculate the steady state (static) flying attitude, we neglect the time dependent terms, to get:

$$\mathbf{K}\,\mathbf{x} + \mathbf{F}_{susp} = \mathbf{F}_{abs}(\mathbf{x}) + \mathbf{F}_{con}(\mathbf{x}) \tag{2}$$

The air-bearing force is calculated by integrating the air-pressure and the shear stress under the slider. The Generalized Reynolds Equation is solved to get the pressure field.

However the spacing between the slider and the disk is extremely small (of the order of a few nanometers, which is much less than the mean free path of air). Under these conditions, the continuum assumption for the air and the no-slip boundary conditions are no longer valid. Hence the Reynolds equation is modified to include rarefaction and slip effects. The modified Generalized Reynolds Equation can be written in the following form in terms of dimensionless variables, $P = p/p_0$ (pressure normalized with respect to the ambient pressure p_0), $H = h/h_m$ (slider-disk clearance normalized with respect to a nominal spacing h_m) and $T = \omega \cdot t$ (time non-dimensionalized with respect to the angular velocity of the disk ω):

$$\nabla \cdot (Q\ PH^3\ \nabla P) = \mathbf{\Lambda} \cdot \nabla(PH) + \tau \frac{\partial}{\partial T}(PH) \tag{3}$$

where $\nabla = \frac{\partial}{\partial X}\mathbf{E}_X + \frac{\partial}{\partial Y}\mathbf{E}_Y$ is the gradient operator with respect to the normalized coordinates $X = x/L$ and $Y = y/L$ where L is a characteristic length scale for the slider. The non-dimensional vector $\mathbf{\Lambda}$ is the bearing number defined as $\mathbf{\Lambda} = \frac{6\mu \mathbf{U}L}{p_0 h_m^2}$, where μ is the dynamic viscosity of air and $\mathbf{U}$ is the local velocity vector of the disk. The squeeze number τ is defined as $\tau = \frac{12\mu\omega L^2}{p_0 h_m^2}$. It represents the ratio of transient effects to the diffusion effects in the problem. The factor Q incorporates the modification to the continuum Reynolds Equation for slip and rarefaction effects. A good discussion of the various models for Q has been given by Wu (2001). Values of the parameter Q for different models are briefly listed in Table 1, where, $a = \frac{2-\alpha}{\alpha}$, α is the accommodation factor, and $K_n = \frac{\lambda}{h_m}$ is the Knudsen number, λ being the mean free path of air. The function $f\left(\frac{K_n}{PH}\right)$ is given by Fukui and Kaneko (1990).

To calculate the steady state pressure distribution over the slider we neglect the time dependent terms to get the steady state generalized Reynolds equation:

$$\nabla \cdot (Q\ PH^3\ \nabla P) = \mathbf{\Lambda} \cdot \nabla(PH) \tag{4}$$

The above equation is solved over the domain of the slider (denoted by $\mathcal{S}$) with the boundary conditions of ambient pressure ($P = 1$) at the edges of the slider to get the pressure distribution over the slider.

To derive the weak form of Eqn. 4, we multiply the equation by a test function v, and integrate over the domain $\mathcal{S}$ to finally get:

$$\int_{\mathcal{S}} \nabla v \cdot (Q\, PH^3\, \nabla P)\, \mathrm{dA} + \int_{\mathcal{S}} v\, \boldsymbol{\Lambda} \cdot \nabla(PH)\, \mathrm{dA} - \int_{\partial \mathcal{S}} v\, (Q\, PH^3\, \nabla P) \cdot \mathbf{n}\, \mathrm{dS} = 0 \qquad (5)$$

The above equation along with the boundary condition $P = 1$ over $\partial \mathcal{S}$ is the weak form of Eqn. 4, and it can be solved to give the pressure field over the slider $\mathcal{S}$. We decompose the domain of the slider $\mathcal{S}$ into the sum of elements, such that:

$$\mathcal{S} = \bigcup_{i=1}^{N_e} \mathcal{T}_i \quad || \ \mathcal{T}_i \cap \mathcal{T}_j = \emptyset \text{ for } i \neq j \qquad (6)$$

Writing the weak form Eqn. 5 over each element $\mathcal{T}_i$, and applying the essential boundary conditions we obtain:

$$\int_{\mathcal{T}_i} \nabla v \cdot (Q\, PH^3\, \nabla P)\, \mathrm{dA} + \int_{\mathcal{T}_i} v\, \boldsymbol{\Lambda} \cdot \nabla(PH)\, \mathrm{dA} - \int_{\partial \mathcal{T}_i \backslash \partial \mathcal{S}} v\, (Q\, PH^3\, \nabla P) \cdot \mathbf{n}\, \mathrm{dS} = 0 \qquad (7)$$

Table 1: Rarefaction and slip models

Model	Flow Factor Q
Continuum model	1
First order slip model	$1 + 6a\frac{K_n}{PH}$
Second order slip model	$1 + 6\frac{K_n}{PH} + 6\left(\frac{K_n}{PH}\right)^2$
Fukui-Kaneko model	$f\left(\frac{K_n}{PH}\right)$

4 The Forward Problem

In the forward problem the objective is to find the pressure distribution given the attitude of the slider. Since the attitude is specified and the slider profile is known, the clearance H over the slider $\mathcal{S}$ is known, thus the only unknown in the problem is P over the slider $\mathcal{S}$.

To solve the nonlinear forward problem by the Newton Raphson method, Eqn. 7 needs to be linearized with respect to the pressure P. Writing $P = P_0 + \partial P$ and retaining only the linear terms in ∂P we get:

$$
\int_{\mathcal{T}_i} \nabla v \cdot (Q \, P_0 H^3 \, \nabla P_0 + Q \, P_0 H^3 \, \nabla \partial P + Q \, \partial P H^3 \, \nabla P_0) \, \mathrm{dA}
$$

$$
+ \int_{\mathcal{T}_i} v \, \mathbf{\Lambda} \cdot (H \, \nabla P_0 + P_0 \, \nabla H + H \, \nabla \partial P + \partial P \, \nabla H) \, \mathrm{dA}
$$

$$
- \int_{\partial \mathcal{T}_i \backslash \partial \mathcal{S}} v \, (Q \, P_0 H^3 \, \nabla P_0 + Q \, P_0 H^3 \, \nabla \partial P + Q \, \partial P H^3 \, \nabla P_0) \cdot \mathbf{n} \, \mathrm{dS} = 0 \quad (8)
$$

For finite element discretization, we use the Streamline Upwind Petrov Galerkin formulation proposed by Brooks and Hughes (1982). Using linear triangular elements with elemental basis functions denoted by ϕ^e for the pressure field and $\widetilde{\phi}^e$ for the test functions we can write:

$$
P = \phi^{eT}\mathbf{P}^e \tag{9}
$$

$$
\nabla P = \mathbf{B}^{eT}\mathbf{P}^e \qquad \text{where } \mathbf{B}^e = \left\{ \frac{\partial \phi_i^e}{\partial X} \quad \frac{\partial \phi_i^e}{\partial Y} \right\} \tag{10}
$$

$$
v = \widetilde{\phi}^{eT}\mathbf{v}^e \tag{11}
$$

$$
\nabla v = \overline{\mathbf{B}}^{eT}\mathbf{v}^e \qquad \text{where } \overline{\mathbf{B}}^e = \left\{ \frac{\partial \widetilde{\phi}_i^e}{\partial X} \quad \frac{\partial \widetilde{\phi}_i^e}{\partial Y} \right\} \tag{12}
$$

Substituting these into Eqn. 8 and rearranging we reduce it to:

$$\mathbf{K}^e\,\partial\mathbf{P}^e - \mathbf{R}^e - \int\limits_{\partial\mathcal{T}_i\backslash\partial\mathcal{S}} \widetilde{\boldsymbol{\phi}}^e\,(Q\;P_0 H^3\;\nabla P_0 + Q\;P_0 H^3\;\mathbf{B}^{eT}\partial\mathbf{P}^e + Q\;\boldsymbol{\phi}^{eT}\partial\mathbf{P}^e H^3\;\nabla P_0)\cdot\mathbf{n}\;\mathrm{dS} = 0 \quad (13)$$

where $\mathbf{K}^e$ and $\mathbf{R}^e$ are the element stiffness matrix and element flux vector defined as:

$$\mathbf{K}^e = \int\limits_{\mathcal{T}_i}(QP_0 H^3\,\overline{\mathbf{B}}^e\mathbf{B}^{eT} + QH^3\,\overline{\mathbf{B}}^e\nabla P_0\,\boldsymbol{\phi}^{eT} + H\,\widetilde{\boldsymbol{\phi}}^e\mathbf{\Lambda}^T\mathbf{B}^{eT} + \widetilde{\boldsymbol{\phi}}^e\mathbf{\Lambda}^T\nabla H\,\boldsymbol{\phi}^{eT})\;\mathrm{dA} \quad (14)$$

$$\mathbf{R}^e = -\int\limits_{\mathcal{T}_i}(QP_0 H^3\,\overline{\mathbf{B}}^e\nabla P_0 + H\,\widetilde{\boldsymbol{\phi}}^e\mathbf{\Lambda}^T\nabla P_0 + P_0\widetilde{\boldsymbol{\phi}}^e\mathbf{\Lambda}^T\nabla H)\;\mathrm{dA} \quad (15)$$

Assembling the elemental equations we obtain the global system of equations:

$$\mathbf{K}\,\partial\mathbf{P} = \mathbf{R} \quad (16)$$

where, $\mathbf{K} = \bigwedge\limits_{i=1}^{N_e}\mathbf{K}^e$, $\partial\mathbf{P} = \bigwedge\limits_{i=1}^{N_e}\partial\mathbf{P}^e$ and $\mathbf{R} = \bigwedge\limits_{i=1}^{N_e}\mathbf{R}^e$, and $\bigwedge$ is the assembly operator.

The above method is implemented as an iterative Newton scheme with line search to ensure rapid convergence. The resulting system of equations obtained at each iteration is sparse, but not ordered and has a large bandwidth (see Fig. 2(a)). In a previous study Dutto (1993) found that the Reverse Cuthill McKee algorithm gives good orderings and results in rapid convergence using the ILU(0) (Incomplete LU with no fill-in) preconditioned GMRES (Generalized Minimum Residual) methods for solving the compressible Navier Stokes equations. Hence we use the Reverse Cuthill McKee algorithm (see Quarteroni, Sacco, and Saleri, 2000) for bandwidth reduction to obtain a banded matrix (as in Fig. 2(b)). The system is then solved using the ILU(0) preconditioned GMRES Method (see Saad, 2003) with adaptive subspace selection.

Once the pressure field over the slider has been determined, the forces and moments about

the pivot location can be calculated by simply integrating the pressures over the elements using the following relations:

$$F_z = \mathbf{C}_{F_z}^T \mathbf{P} \qquad \text{where } \mathbf{C}_{F_z} = p_0 L^2 \overset{N_e}{\underset{i=1}{\mathbb{A}}} \int_{\mathcal{T}_i} \boldsymbol{\phi}^e \, \mathrm{dA} \qquad (17)$$

$$M_{pitch} = \mathbf{C}_{M_{pitch}}^T \mathbf{P} \qquad \text{where } \mathbf{C}_{M_{pitch}} = p_0 L^3 \overset{N_e}{\underset{i=1}{\mathbb{A}}} \int_{\mathcal{T}_i} X \boldsymbol{\phi}^e \, \mathrm{dA} \qquad (18)$$

$$M_{roll} = \mathbf{C}_{M_{roll}}^T \mathbf{P} \qquad \text{where } \mathbf{C}_{M_{roll}} = p_0 L^3 \overset{N_e}{\underset{i=1}{\mathbb{A}}} \int_{\mathcal{T}_i} Y \boldsymbol{\phi}^e \, \mathrm{dA} \qquad (19)$$

5   Inverse problem

In the inverse problem the net forces and moments on the slider are known and the pressure distribution and the flying attitude of the slider are to be determined. The inverse problem can be solved in either of two ways, 1) by linearizing Eqn. 2 and solving a series of forward problems, or, 2) by linearizing Eqn. 7 along with Eqn. 2 and solving the resulting system. The first method requires two levels of iterations, the first one to solve the linearized version of Eqn. 2 and the second level to solve the forward problem at each of iteration. The second method, on the other hand, requires just one level of iteration, which however is more difficult to solve and takes longer to converge.

The first method solves a series of forward problems. Linearizing the governing equation Eqn. 2 about $\mathbf{x}_0$, we get the following equation:

$$\mathbf{K} \, \partial \mathbf{x} - \mathbf{K}_{abs} \, \partial \mathbf{x} + \mathbf{K}_{con} \, \partial \mathbf{x} = \mathbf{F}_{abs}(\mathbf{x}_0) + \mathbf{F}_{con}(\mathbf{x}_0) - \mathbf{K} \, \mathbf{x} - \mathbf{F}_{susp} \qquad (20)$$

where $\mathbf{K}_{abs}$ and $\mathbf{K}_{con}$ are the air-bearing and contact stiffnesses of the slider-disk interface. Equation 20 can be formulated in an iterative form, and the solution of the resulting problem

8

involves solving the forward problem (at $\mathbf{x}_0$) along with the calculation of the air-bearing stiffness matrix. Solution of the forward problem has already been discussed in the previous section.

To perform the air bearing stiffness calculation we observe that the clearance H depends on the attitude of the slider as:

$$H = \frac{1}{h_m} \left(d_{etch} + z_{pivot} + XL \cdot \theta_{pitch} + YL \cdot \theta_{roll} \right) \tag{21}$$

where d_{etch} is the etch depth, z_{pivot} is the z-height of the pivot location, θ_{pitch} is the pitch angle and θ_{roll} is the roll angle, and X and Y are the coordinates of the point measured from the pivot location (see Fig. 1). Writing the weak form of the time-independent Generalized Reynolds equation, Eqn. 5 as:

$$\vartheta(P, H) = 0 \tag{22}$$

then differentiating with respect to z_{pivot} and rearranging, we get:

$$\frac{\mathrm{d}P}{\mathrm{d}z_{pivot}} = \left[\frac{\partial \vartheta(P, H)}{\partial P} \right]^{-1} \left\{ \frac{\partial \vartheta(P, H)}{\partial H} \cdot \frac{\partial H}{\partial z_{pivot}} \right\} \tag{23}$$

Similarly, differentiating with respect to θ_{pitch} and θ_{roll}, we obtain:

$$\frac{\mathrm{d}P}{\mathrm{d}\theta_{pitch}} = \left[\frac{\partial \vartheta(P, H)}{\partial P} \right]^{-1} \left\{ \frac{\partial \vartheta(P, H)}{\partial H} \cdot \frac{\partial H}{\partial \theta_{pitch}} \right\} \tag{24}$$

$$\frac{\mathrm{d}P}{\mathrm{d}\theta_{roll}} = \left[\frac{\partial \vartheta(P, H)}{\partial P} \right]^{-1} \left\{ \frac{\partial \vartheta(P, H)}{\partial H} \cdot \frac{\partial H}{\partial \theta_{roll}} \right\} \tag{25}$$

Substituting the finite element interpolations and evaluating the expressions above, we get:

$$\left\{ \frac{d\mathbf{P}}{dz_{pivot}} \right\} = \left[\mathbf{K} \right]^{-1} \left\{ \frac{\partial \mathbf{R}}{\partial z_{pivot}} \right\} \tag{26}$$

$$\left\{ \frac{d\mathbf{P}}{d\theta_{pitch}} \right\} = \left[\mathbf{K} \right]^{-1} \left\{ \frac{\partial \mathbf{R}}{\partial \theta_{pitch}} \right\} \tag{27}$$

$$\left\{ \frac{d\mathbf{P}}{d\theta_{roll}} \right\} = \left[\mathbf{K} \right]^{-1} \left\{ \frac{\partial \mathbf{R}}{\partial \theta_{roll}} \right\} \tag{28}$$

where $\mathbf{K}$ is the global stiffness matrix and the righthand side vectors are defined as:

$$\left\{ \frac{\partial \mathbf{R}}{\partial z_{pivot}} \right\} = -\frac{1}{h_m} \overset{N_e}{\underset{i=1}{A}} \int_{\mathcal{T}_i} (3\, Q P_0 H^2\, \overline{\mathbf{B}}^e \nabla P_0 + \widetilde{\boldsymbol{\phi}}^e \boldsymbol{\Lambda}^T \nabla P_0)\, \mathrm{dA} \tag{29}$$

$$\left\{ \frac{\partial \mathbf{R}}{\partial \theta_{pitch}} \right\} = -\frac{L}{h_m} \overset{N_e}{\underset{i=1}{A}} \int_{\mathcal{T}_i} (3\, Q P_0 H^2\, \overline{\mathbf{B}}^e \nabla P_0 + \widetilde{\boldsymbol{\phi}}^e \boldsymbol{\Lambda}^T \nabla P_0) \cdot X\, \mathrm{dA} \tag{30}$$

$$\left\{ \frac{\partial \mathbf{R}}{\partial \theta_{roll}} \right\} = -\frac{L}{h_m} \overset{N_e}{\underset{i=1}{A}} \int_{\mathcal{T}_i} (3\, Q P_0 H^2\, \overline{\mathbf{B}}^e \nabla P_0 + \widetilde{\boldsymbol{\phi}}^e \boldsymbol{\Lambda}^T \nabla P_0) \cdot Y\, \mathrm{dA} \tag{31}$$

The terms of the 3×3 stiffness matrix can then be evaluated as:

$$\mathbf{K}_{abs} = \begin{bmatrix} \mathbf{C}_{F_z}^T \left\{ \frac{\partial \mathbf{R}}{\partial z_{pivot}} \right\} & \mathbf{C}_{M_{pitch}}^T \left\{ \frac{\partial \mathbf{R}}{\partial z_{pivot}} \right\} & \mathbf{C}_{M_{roll}}^T \left\{ \frac{\partial \mathbf{R}}{\partial z_{pivot}} \right\} \\ \mathbf{C}_{F_z}^T \left\{ \frac{\partial \mathbf{R}}{\partial \theta_{pitch}} \right\} & \mathbf{C}_{M_{pitch}}^T \left\{ \frac{\partial \mathbf{R}}{\partial \theta_{pitch}} \right\} & \mathbf{C}_{M_{pitch}}^T \left\{ \frac{\partial \mathbf{R}}{\partial \theta_{pitch}} \right\} \\ \mathbf{C}_{F_z}^T \left\{ \frac{\partial \mathbf{R}}{\partial \theta_{roll}} \right\} & \mathbf{C}_{M_{pitch}}^T \left\{ \frac{\partial \mathbf{R}}{\partial \theta_{roll}} \right\} & \mathbf{C}_{M_{roll}}^T \left\{ \frac{\partial \mathbf{R}}{\partial \theta_{roll}} \right\} \end{bmatrix} \tag{32}$$

Thus the stiffness is obtained by the solution of three extra linear systems. However this is not computationally very expensive even with iterative methods (where the system matrix $\mathbf{K}$ has not been factorized) since preconditioners for $\mathbf{K}$ will already have been evaluated.

The equation of motion is now solved using the Newton Raphson method by repeatedly solving the linearized equation, Eqn. 37. The forward problem is solved at each iteration. Again we use line search to speed up convergence of the iterations. Stiffness calculations

for the air bearing are made after every few iterations (and when line-search fails) with symmetric Broyden updates of rank-2 after each iteration. This avoids wasting too much time on calculating the stiffness matrix at each iteration, while still maintaining a good approximation of the stiffness matrix at each iteration.

The second method for solving the inverse problem is to linearize the governing equation, Eqn. 2, and the Reynolds equation together, and then solve only one level of iterations.

Consider again the elemental weak form of the Generalized Reynolds equation, Eqn. 7. Linearizing with respect to $\{P, H\}$ about $\{P_0, H_0\}$, we get:

$$
\int_{\mathcal{T}_i} \nabla v \cdot (Q\ P_0 H_0^3\ \nabla P_0 + Q\ P_0 H_0^3\ \nabla \partial P + Q\ \partial P H_0^3\ \nabla P_0 + 3Q\ P_0 H_0^2\ \partial H\ \nabla P_0)\ \mathrm{dA}
$$

$$
+ \int_{\mathcal{T}_i} v\ \mathbf{\Lambda} \cdot (H_0\ \nabla P_0 + P_0\ \nabla H_0 + H_0\ \nabla \partial P + \partial P\ \nabla H_0 + \partial H\ \nabla P_0 + P_0\ \nabla \partial H)\ \mathrm{dA}
$$

$$
- \int_{\partial \mathcal{T}_i \backslash \partial \mathcal{S}} v\ (Q\ P_0 H_0^3\ \nabla P_0 + Q\ P_0 H_0^3\ \nabla \partial P + Q\ \partial P H_0^3\ \nabla P_0 + 3Q\ P_0 H_0^2\ \partial H\ \nabla P_0) \cdot \mathbf{n}\ \mathrm{dS} = 0
$$

$$(33)$$

which is referred to as the 'fully linearized' form of the elemental weak form.

Substituting the discrete forms of the pressure and the test functions, we obtain:

$$
\int_{\mathcal{T}_i} \left(\overline{\mathbf{B}}^{eT} \mathbf{v}^e \right)^T (Q\ P_0 H_0^3\ \nabla P_0 + Q\ P_0 H_0^3\ \mathbf{B}^{eT} \partial \mathbf{P}^e + Q\ \boldsymbol{\phi}^{eT} \partial \mathbf{P}^e H_0^3\ \nabla P_0 + 3Q\ P_0 H_0^2\ \partial H\ \nabla P_0)\ \mathrm{dA}
$$

$$
+ \int_{\mathcal{T}_i} \widetilde{\boldsymbol{\phi}}^{eT} \mathbf{v}^e\ \mathbf{\Lambda} \cdot (H_0\ \nabla P_0 + P_0\ \nabla H_0 + H_0\ \mathbf{B}^{eT} \partial \mathbf{P}^e + \boldsymbol{\phi}^{eT} \partial \mathbf{P}^e\ \nabla H + \partial H\ \nabla P_0 + P_0\ \nabla \partial H_0)\ \mathrm{dA}
$$

$$
- \int_{\partial \mathcal{T}_i \backslash \partial \mathcal{S}} \widetilde{\boldsymbol{\phi}}^{eT} \mathbf{v}^e\ (Q\ P_0 H_0^3\ \nabla P_0 + Q\ P_0 H_0^3\ \mathbf{B}^{eT} \partial \mathbf{P}^e + Q\ \boldsymbol{\phi}^{eT} \partial \mathbf{P}^e H_0^3\ \nabla P_0 + 3Q\ P_0 H_0^2\ \partial H_0\ \nabla P_0) \cdot \mathbf{n}\ \mathrm{dS} = 0
$$

$$(34)$$

11

Now using the definition of H in Eqn. 21, we can rewrite ∂H and $\nabla \partial H$ as:

$$\partial H = \mathbf{C}_H^T \partial \mathbf{x} \qquad \text{where } \mathbf{C}_H = \frac{1}{h_m} \left\{ \begin{array}{ccc} 1 & X \cdot L & Y \cdot L \end{array} \right\}^T \tag{35}$$

$$\nabla \partial H = \mathbf{C}_{\nabla H}^T \partial \mathbf{x} \qquad \text{where } \mathbf{C}_{\nabla H} = \frac{L}{h_m} \left[\begin{array}{ccc} 0 & 1 & 0 \\ 0 & 0 & 1 \end{array} \right]^T \tag{36}$$

Substituting this into Eqn. 34, we obtain:

$$\mathbf{K}_{full}^e \left\{ \begin{array}{cc} \partial \mathbf{P}^{eT} & \partial \mathbf{x}^T \end{array} \right\}^T - \mathbf{R}_{full}^e -$$

$$\int_{\partial \mathcal{T}_i \setminus \partial \mathcal{S}} \widetilde{\boldsymbol{\phi}}^e \ (Q \ P_0 H_0^3 \ \nabla P_0 + Q \ P_0 H_0^3 \ \mathbf{B}^{eT} \partial \mathbf{P}^e + Q \ \boldsymbol{\phi}^{eT} \partial \mathbf{P}^e H_0^3 \ \nabla P_0 + 3Q \ P_0 H_0^2 \ \partial H \ \nabla P_0) \cdot \mathbf{n} \ \mathrm{dS} = 0$$

$$\tag{37}$$

where $\mathbf{K}_{full}^e$ and $\mathbf{R}_{full}^e$ are the element stiffness matrix and element flux vector defined as:

$$\mathbf{K}_{full}^e = \left[\begin{array}{cc} \mathbf{K}_P^e & \mathbf{K}_H^e \end{array} \right] \tag{38}$$

$$\mathbf{K}_P^e = \int_{\mathcal{T}_i} (Q \ P_0 H_0^3 \ \overline{\mathbf{B}}^e \mathbf{B}^{eT} + Q \ H_0^3 \ \overline{\mathbf{B}}^e \nabla P_0 \ \boldsymbol{\phi}^{eT} + H_0 \ \widetilde{\boldsymbol{\phi}}^e \boldsymbol{\Lambda}^T \mathbf{B}^{eT} + \widetilde{\boldsymbol{\phi}}^e \boldsymbol{\Lambda}^T \nabla H \ \boldsymbol{\phi}^{eT}) \ \mathrm{dA}$$

$$\mathbf{K}_H^e = \int_{\mathcal{T}_i} (3Q \ P_0 H_0^2 \ \overline{\mathbf{B}}^e \mathbf{B}^{eT} \nabla P_0 \ \mathbf{C}_H + \widetilde{\boldsymbol{\phi}}^e \boldsymbol{\Lambda}^T \nabla P_0 \ \mathbf{C}_H + P_0 \ \widetilde{\boldsymbol{\phi}}^e \boldsymbol{\Lambda}^T \ \mathbf{C}_{\nabla H}) \ \mathrm{dA}$$

$$\mathbf{R}_{full}^e = - \int_{\mathcal{T}_i} (Q P_0 H_0^3 \ \overline{\mathbf{B}}^e \nabla P_0 + H_0 \ \widetilde{\boldsymbol{\phi}}^e \boldsymbol{\Lambda}^T \nabla P_0 + P_0 \widetilde{\boldsymbol{\phi}}^e \boldsymbol{\Lambda}^T \nabla H_0) \ \mathrm{dA} \tag{39}$$

After assembling the set of equations in Eqn. 37, we get a system of N_n equations in $N_n + 3$ unknowns. We need 3 more equations to determine the solution of the system. These three equations are the linearized governing equations (Eqn. 20) in the z_{pivot}, θ_{pitch} and θ_{roll}

directions. Thus we end up with the following system of equations:

$$\begin{bmatrix} \mathbf{K}_P & \mathbf{K}_H \\ \mathbf{C}_{abs} & \mathbf{K}_{eff} \end{bmatrix} \begin{Bmatrix} \partial \mathbf{P} \\ \partial \mathbf{x} \end{Bmatrix} = \begin{Bmatrix} \mathbf{R}_{full} \\ \mathbf{R}_H \end{Bmatrix} \tag{40}$$

where $\mathbf{K}_H = \overset{N_e}{\underset{i=1}{\mathbb{A}}} \mathbf{K}_H^e$, $\mathbf{R}_{full} = \overset{N_e}{\underset{i=1}{\mathbb{A}}} \mathbf{R}_{full}^e$, $\mathbf{C}_{abs} = \begin{Bmatrix} \mathbf{C}_{F_z} & \mathbf{C}_{M_{pitch}} & \mathbf{C}_{M_{roll}} \end{Bmatrix}$, $\mathbf{K}_{eff} = \mathbf{K}_{susp} + \mathbf{K}_{abs} + \mathbf{K}_{con}$ and $\mathbf{R}_H = \mathbf{C}_{abs}^T \mathbf{P}_0 + \mathbf{F}_{con}(\mathbf{x}_0) - \mathbf{K}_{susp}\mathbf{x}_0 - \mathbf{F}_{susp}$.

The formulation described above is again implemented using a Newton Raphson iterative scheme. The resulting system of equations at each iteration is also sparse, however the equations corresponding to the balance of forces/moments are full and the coefficients corresponding to the slider attitude are nonzero for all of the equations. Hence after the application of the Reverse Cuthill McKee algorithm, we end up with an 'arrowhead' matrix (see Fig. 2(c)). For simplicity, the arrowhead matrix is also solved using the preconditioned GMRES algorithm used for the forward problem and the inverse problem solved using method 1. The method is found to be slower than method 1 using this algorithm, however it is expected to be faster using either a direct method or a preconditioner that exploits the structure of the matrix.

For the analysis to be carried out in the subsequent sections, we define a new norm: the *force* norm. The force norm is a weighted norm that can be directly used to correlate fields (pressures etc.) to their integrals over the domain $\mathcal{S}$ (forces etc.). The force norm is defined as:

$$|\boldsymbol{\zeta}|_F = p_0 L^2 \sum_{j=1}^{N_e} \int_{T_j} |\zeta_i| \, \phi_i^e \, \mathrm{d}A \approx \mathbf{C}_{F_z}^T |\boldsymbol{\zeta}| \tag{41}$$

13

6   Numerical Simulations

Meshes for the sliders are generated using *TRIANGLE*, a robust 2D triangular mesh generator developed by Shewchuk (1996). In order to ensure that errors in the solutions are small, the mesh is automatically refined based on certain criteria. Refinement and regeneration of the meshes is also done using *TRIANGLE*. The coarsest level meshes are generated such that the element edges conform to the slider's rail and wall geometries. Coarse level meshes for two slider designs are shown in Fig. 3. Various criteria for refinement are investigated later in this section. Refined meshes are nested within the coarse mesh, hence they conform to the slider geometry as well.

The formulations described above were implemented in C++ and studies were carried out to investigate grid convergence.

6.1   Forward problem

The slider 1 design is simulated to study convergence for increasing grid sizes. The operational parameters are fixed at a nominal fly-height of 20 nm, pitch of 200 μrad, roll of 1 μrad and flying over a disk spinning at an RPM of 10K at a radius of 32 mm with 0° skew. The grid used for each of the meshes is a uniform triangular grid.

Figure 4 shows plots of the resultant pressure force and pitch-moment for slider 1. In Fig. 5, we plot the error at each level. The error is computed by calculating the pressure profile at a very fine grid and treating it as the exact solution. Data points for fine meshes are neglected since they appear to be too close to the mesh used for calculating the error. We see that the order of accuracy is close to 1.1 for both the force and the pitch-moment. The pressure profile for slider 1 can be seen in Fig. 6. No large pressure gradients are observed and hence an order of convergence of 1.5 is observed numerically.

By considering other designs we find that the order of convergence of the solution for our

problem is strongly dependent on the slider geometry and the operating parameters of the slider. However the grid convergence discussed in this section is for a uniform mesh. We can artificially enhance grid convergence by using selective mesh refinement to refine only areas of the slider where the error is high.

Next we will study various refinement strategies for the mesh so as to obtain the most accurate solution with the fewest number of nodes.

Pressure based refinement

The value of the steady state pressure can be used as a refinement criterion to refine the coarse level mesh. This leads to the mesh being refined in areas with higher pressures. The rationale behind using this refinement scheme is that areas with higher pressures contribute more to the forces and moments and hence need to be resolved more accurately than regions with lower pressures.

$$\theta_{pres} = \int_{\mathcal{T}_i} |P| \, \mathrm{dA} \tag{42}$$

Clearance based refinement

The clearance under the slider at the steady state can be used as a refinement criterion to refine the coarse level mesh. Thus areas which are closer to the disk (rails and areas closer to the trailing edge) will have a finer mesh than other areas. The rationale here is that areas closer to the disk typically have high pressure and may have higher errors.

$$\theta_{spacing} = \frac{1}{\int_{\mathcal{T}_i} H \, \mathrm{dA}} \tag{43}$$

Pressure gradient based refinement

The pressure gradient under the slider at the steady state can be used as a refinement criterion to refine the coarse level mesh. Thus areas which have large pressure gradients

(typically near the trailing edge pads on the slider) will have a finer mesh than other areas.

$$\theta_{\nabla P} = \int\limits_{\mathcal{T}_i} |\nabla P| \, \mathrm{dA} \tag{44}$$

Flux jump based refinement

The pressure flux jumps under the slider at the steady state can also be used as a refinement criterion to refine the coarse level mesh. In some sense this measure is representative of the interpolation error of the solution. Thus areas which have large pressure flux discontinuities will have a finer mesh than other areas. We observe that the flux jump terms across the elements were neglected during the assembly of the system equations and hence a larger flux jump term may be an indicator of larger error.

$$\theta_{[|\nabla P|]} = \left| h_i \left(\nabla P^+ - \nabla P^- \right) \cdot \mathbf{n} \right| \tag{45}$$

Streamwise clearance gradient based refinement

Next we can also use the streamwise clearance gradient of the slider at the steady state as a refinement criterion to refine the coarse level mesh. Thus areas which have steep clearance gradients (such as on the walls) will have a finer mesh than other areas.

$$\theta_{\nabla H \cdot \lambda} = \int\limits_{\mathcal{T}_i} \frac{|\mathbf{\Lambda} \cdot \nabla H|}{|\mathbf{\Lambda}|} \, \mathrm{dA} \tag{46}$$

Residual based refinement

Finally we explore the strategy wherein the residual of the nonlinear Reynolds equation is used as a refinement criterion to refine the coarse level mesh. Thus areas with higher

residuals are used as an indication of higher error and to generate refined meshes.

$$\theta_{R_e} = \int\limits_{\mathcal{T}_i} |R^e_{n+1}| \, \mathrm{dA} \tag{47}$$

In Figs. 7 and 8, we plot the grid convergence for slider 1 (shown in Fig. 3(a)) and slider 2 (shown in Fig. 3(b)), respectively. We see that convergence is most rapid when the pressure gradient and the flux jumps are used as refinement criteria. Convergence is slower when the residual and streamwise clearance gradient are used as criteria. Convergence is slowest when pressure is used as a refinement criterion. However when the clearance is used as a refinement criterion, the solution does not converge to the correct value for the grid sizes simulated. This is because errors towards the leading edge of the slider do not get reduced quickly enough. We observed that most of the error is concentrated in regions of high pressure gradients, which is often found in areas with steep clearance gradients, such as along walls of rails, and more so towards the trailing edge. With further investigation we find that convergence can be enhanced by generating an initial mesh that has smaller elements near the walls as compared to on top of the rails. This concept will be further investigated next.

6.2 Inverse problem

Three slider designs are simulated for the inverse problem. These are Slider 1, shown in Fig. 3(a), Slider 2 is shown in Fig. 3(b) and Slider 3 which is shown in Fig. 3(c). The operating parameters of the three designs are listed in Table 2. The initial grid used for each of the designs is obtained by the dense-edge strategy described above to ensure rapid convergence, wherein the refinement after each level is uniform. The flying attitude, i.e. the nominal fly-height, the pitch and the roll are plotted for each case.

17

Figure. 9 shows plots of the convergence for slider 1 of the fly height, pitch and the roll with reducing grid sizes. We see that the result obtained from the coarsest mesh is within half a nanometer of the final converged value. Similarly the pitch is found to be within 2 μrad and roll within 0.2 μrad. In Fig. 10 we show plots of the three mesh levels used for the convergence study.

Similarly, attitude convergence plots for the inverse problem shown in Fig. 11 and Fig. 12 for sliders 2 and 3 in Figs. 3(b) and 3(c), respectively. For slider 2, the nominal FH is within 0.2 nm and the pitch and roll are within 2 μrad and 0.2 μrad of the final converged values, respectively. For slider 3, the nominal FH is within 0.2 nm and the pitch and roll are within 3 μrad and 0.3 μrad of the final converged values, respectively.

Table 2: Slider operation parameters for grid convergence studies

	Slider 1	Slider 2	Slider 3
Gram load (g)	1.5	2.0	3.0
PSA (rad)	0.1	0.0	0.0
RSA (rad)	0.0	0.0	0.0
Radius (mm)	32	32	27
Skew (°)	0.0	3.2	-17.5
RPM	10K	7.2K	7.2K

7   Summary and Conclusions

In this paper, we presented a novel method of solving the inverse problem for air-bearing sliders in hard disk drives. We started from basic principles and derived the weak form for the Reynolds equation. The linearization scheme for the governing equations was presented next. First the traditional method was presented wherein the equation of motion is linearized first with respect to the slider attitude and the Reynolds equation is linearized with respect to the pressure. This leads to two levels of iterations for the solution of steady state fly

height of the slider. We also presented the new method where the equation of motion and the Reynolds equation are linearized together with respect to both slider attitude and the pressure. This leads to a single level of iteration.

The formulation is implemented and convergence studies are carried out for the method. The order of convergence is found to depend on the geometry of the slider and the resulting pressure profile that develops under it. Finally we explore various strategies for mesh refinement so as to obtain converged results with a minimum number of nodes. Three different slider designs are investigated and refinements based on flux jumps and pressure gradients are found to work better than other strategies. We also find that the number of levels required for convergence can be reduced if the initial mesh is generated so as to have a fine mesh along rail walls.

Acknowledgment

References

A. N. Brooks and T. J. R. Hughes. Streamline Upwind/Petrov-Galerkin formulations for convection dominated flows with particular emphasis on the incompressible navier-stokes equations. *Computer methods in applied mechanics and engineering*, 32:199–259, 1982.

V. Castelli and J. Pirvics. Review of numerical methods in gas bearing film analysis. *ASME Journal of Lubrication Technology*, 90:777–792, 1968.

E. Cha and D.B. Bogy. A numerical scheme for static and dynamic simulation of subambient pressure shaped rail sliders. *Journal of Tribology, Transactions of the ASME*, 117:36–43, 1995.

D.H. Choi and S.J. Yoon. Static analysis of flying characteristics of the head slider by using an optimization technique. *ASME Journal of Tribology*, 116:90–94, 1994.

L. C. Dutto. The effect of ordering on preconditioned GMRES algorithm, for solving the compressible Navier-Stokes equations. *International Journal for Numerical Methods in Engineering*, 36:457–497, 1993.

S. Fukui and R. Kaneko. A database for interpolation of Poiseuille flow rates for high knudsen number lubrication problems. *Trans. ASME Jounal of Tribology*, 112:78–83, 1990.

C. Garcia-Suarez, D.B. Bogy, and F.E. Talke. Use of an upwind finite element scheme for air bearing calculations. *Tribology and Mechanics of Magnetic Storage Systems*, 1:90–96, 1984.

F. Hendricks. A design tool for steady state gas bearings using finite elements, the apl language and Delaunay Triangulation. *ASLE Tribology and Mechanics of Magnetic Storage Systems*, 5:124–129, 1988.

P. Holani and S. Müftü. An adaptive finite element strategy for analysis of air lubrication in the head-disk interface of a hard disk drive. *Revue Europenne des lment Finis*, 14: 155–180, 2005.

Y. Hu and D. B. Bogy. The cml air bearing dynamic simulator. Technical Report 1995-011, CML, University of California, Berkeley, 1995.

M. Kubo, Y. Ohtsubo, N. Kawashima, and H. Marumo. Finite element solution for the rarefied gas lubrication problem. *Journal of Tribology, Transactions of the ASME*, 110(2): 335–341, 1988.

D.K. Miu and D.B. Bogy. Dynamics of gas-lubricated slider bearing in magnetic recording disk files part ii: Numerical simulation. *Journal of Tribology, Transactions of the ASME*, 108:589–593, 1986.

K. Ono. Dynamic characteristics of the air-lubricated slider bearing for non-contact magnetic recording. *ASME Journal of Lubrication Technology*, 97:250–260, 1972.

J.P. Peng and C.E. Hardie. A finite element scheme for determining the shaped rail slider flying characteristics with experimental confirmation. *Trans. ASME Jounal of Tribology*, 117:358–364, 1995.

A. Quarteroni, R. Sacco, and F. Saleri. *Numerical Analysis*. Springer, 2000.

O.J. Ruiz and D.B. Bogy. A numerical simulation of the head-disk assembly in magnetic hard disk files: Part 1 - component models. *Journal of Tribology, Transactions of the ASME*, 112:593–602, 1990.

Y. Saad. *Iterative Methods for Sparse Linear Systems*. SIAM, 2003.

J. R. Shewchuk. Triangle: Engineering a 2D Quality Mesh Generator and Delaunay Triangulator. In Ming C. Lin and Dinesh Manocha, editors, *Applied Computational Geometry:*

Towards Geometric Engineering, volume 1148 of *Lecture Notes in Computer Science*, pages 203–222. Springer-Verlag, May 1996. From the First ACM Workshop on Applied Computational Geometry.

P. W. Smith, M. H. Wahl, and F. E. Talke. Accelerated natural convergence for pivoted slider bearings. *Tribology Transactions*, 38(3):595–600, 1995.

T. Tang. Dynamics of air-lubricated slider bearings for non-contact magnetic recording. *ASME Journal of Lubrication Technology*, 93(2):272–278, 1972.

J. W. White and A. Nigam. A factored implicit scheme for the numerical solution of the reynolds equation at very low spacing. *ASME Journal of Lubrication Technology*, 102: 80–85, 1980.

L. Wu. *Physical Modeling and Numerical Simulations of the Slider Air Bearing Problem of Hard disk drives.* PhD thesis, University of California, Berkeley, 2001.

L. Wu and D. B. Bogy. Unstructured adaptive triangular mesh generation techniques and finite volume schemes for the air bearing problem in hard disk drives. *ASME Journal of Tribology*, 122:761–770, 2000.

H. Yamaura and K. Ono. Inverse analysis of flying height slider bearings for magnetic disk recording. *Proceedings of the Japan Int. Trib. Conf., Nagoya*, pages 1917–1922, 1990.

8 Figures
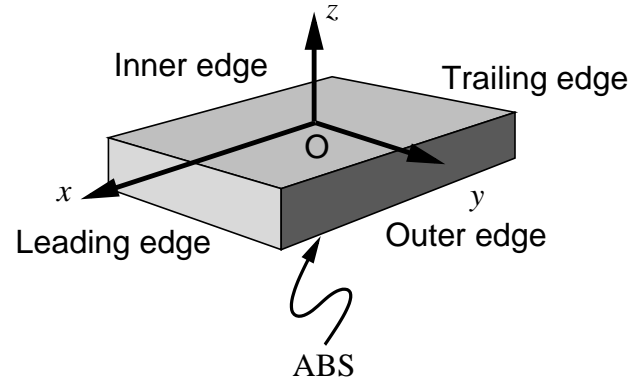
Figure 1: System Coordinate System
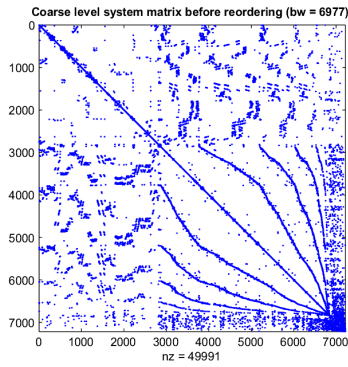
(a) Before node reordering for forward problem
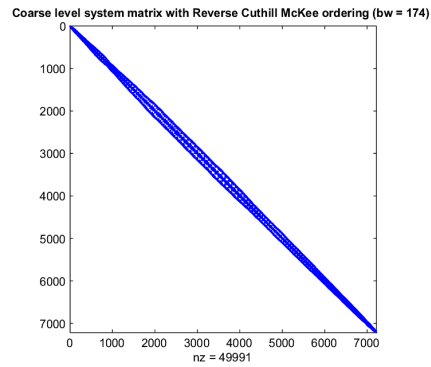
(b) After RCM ordering for forward problem
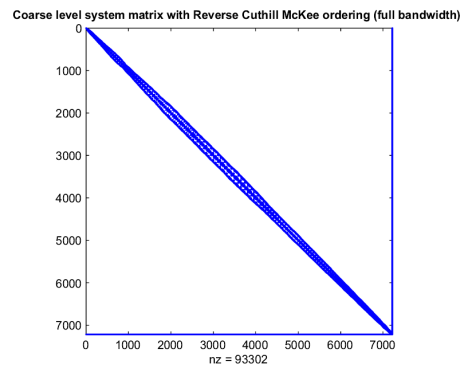
(c) After RCM ordering for Method 2 (Note: the last 3 rows and columns are full)

Figure 2: Coarse level system matrix fill pattern

24
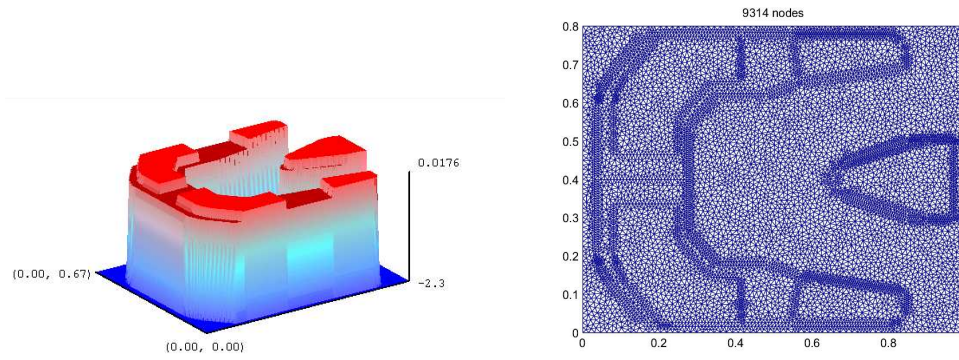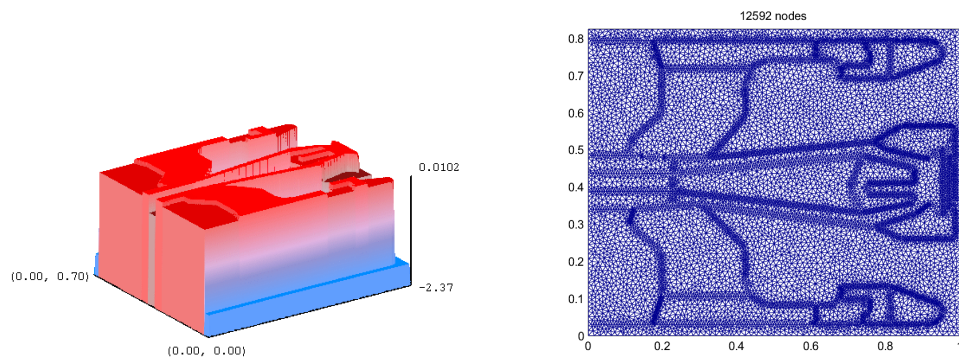
(a) Slider 1

(b) Slider 2
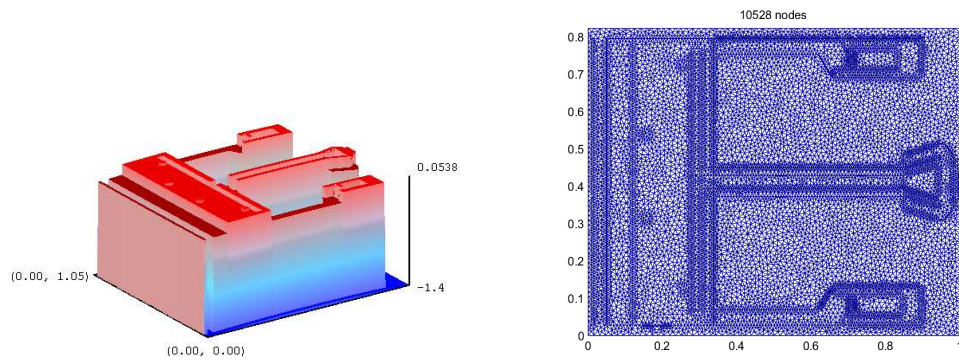
(c) Slider 3

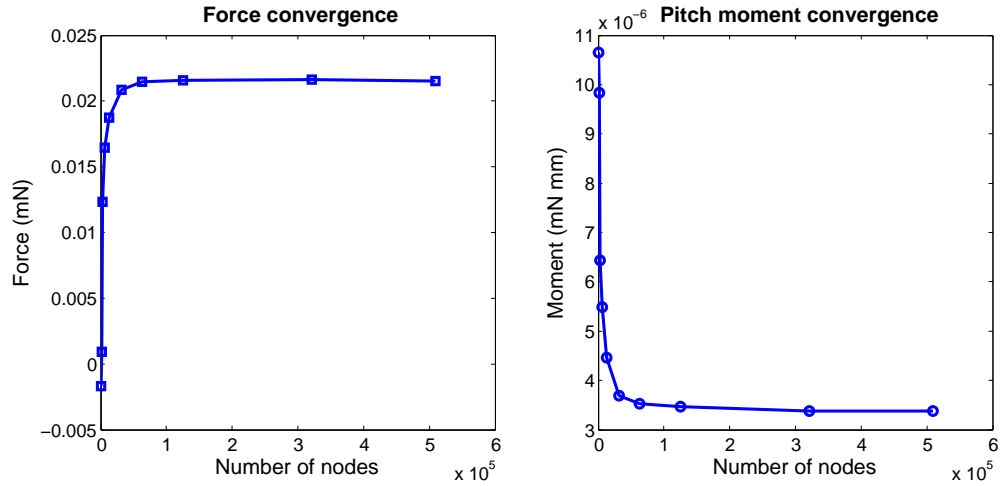Figure 3: Slider designs and coarse level meshes used for simulations
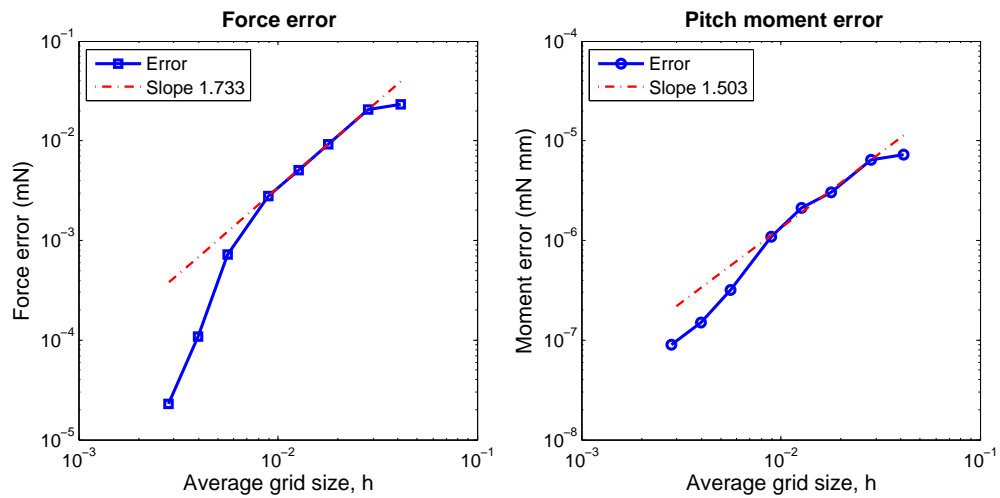
25

Figure 4: Grid convergence for slider 1 forward problem

Figure 5: Force error for slider 1 forward problem
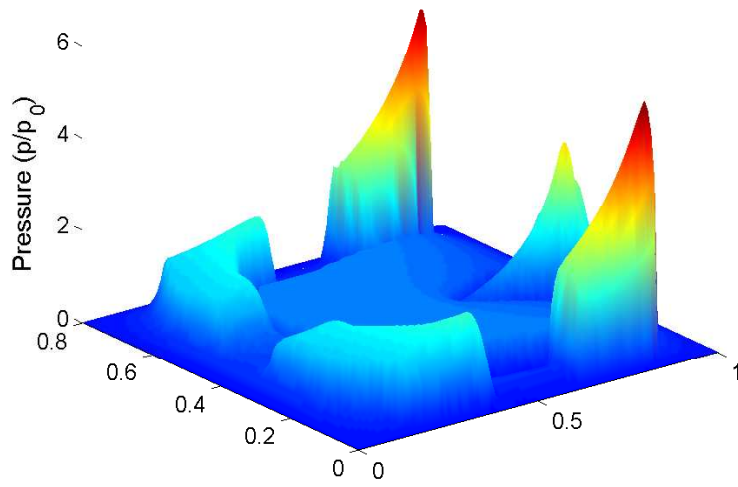
Figure 6: Converged pressure profile for slider 1
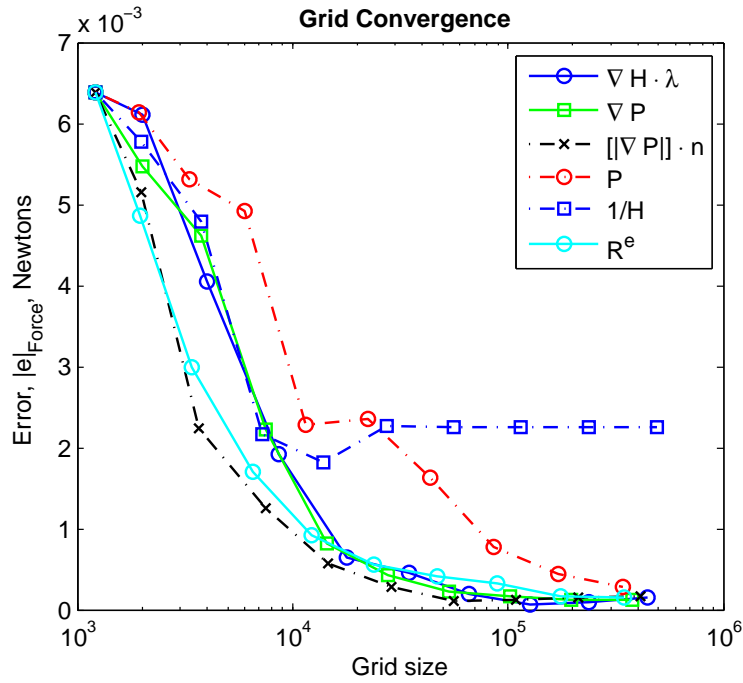
Figure 7: Grid convergence for slider 1 using various refinement strategies
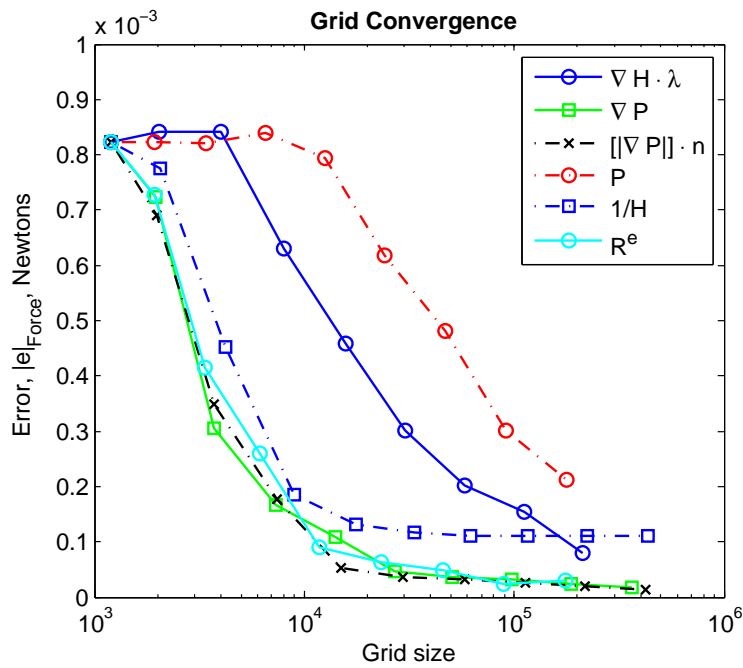
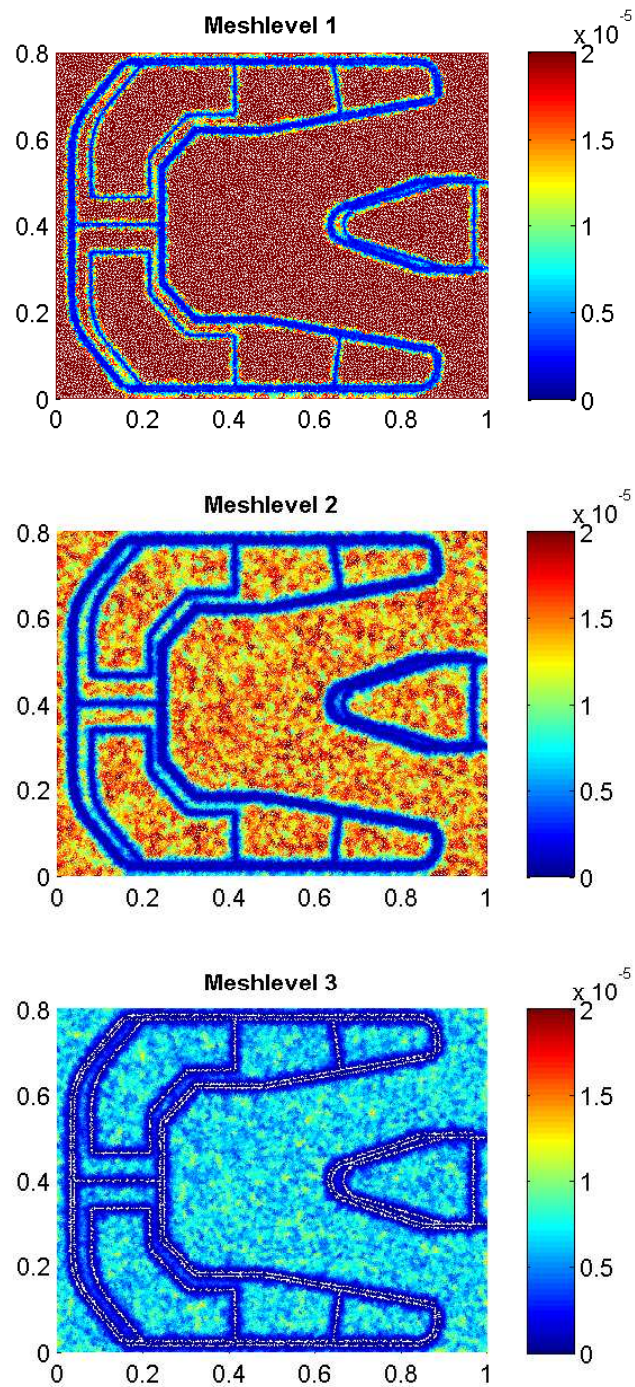Figure 8: Grid convergence for slider 2 using various refinement strategies
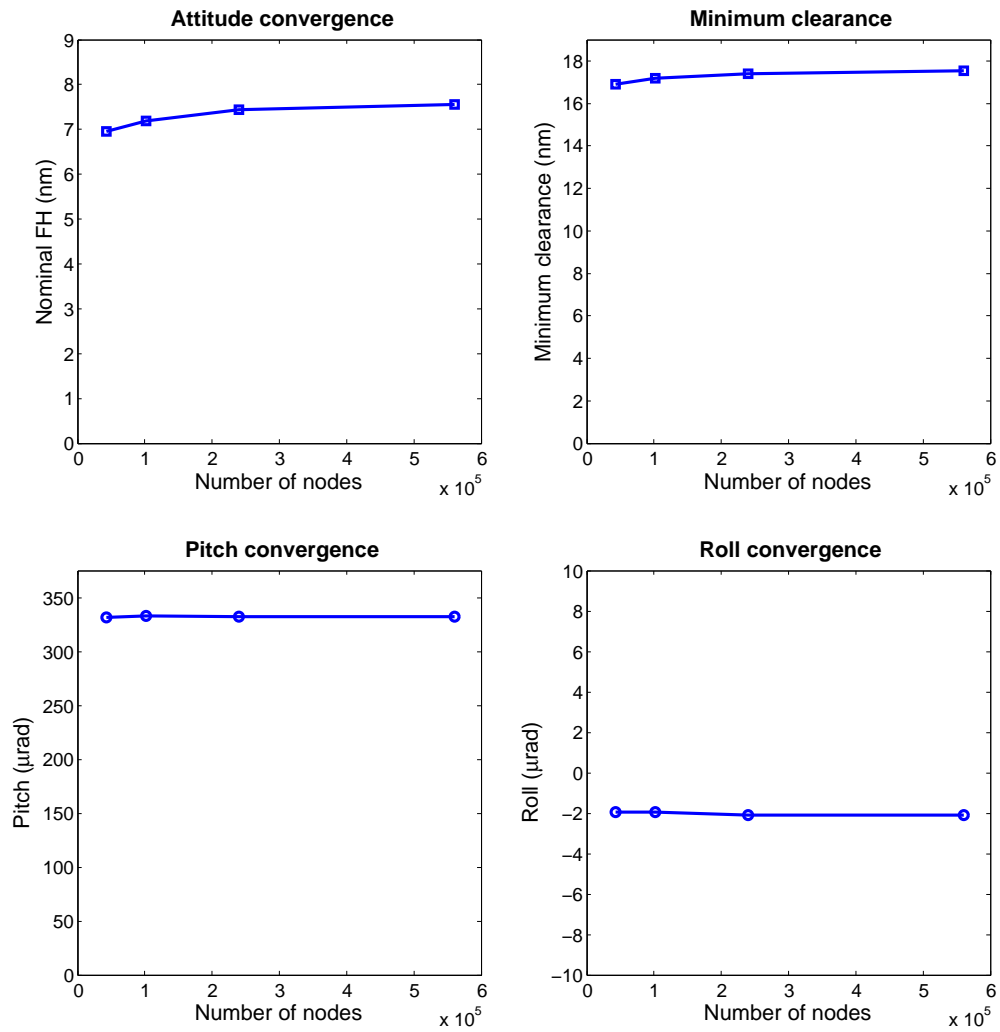
Figure 9: Grid convergence for slider 1 inverse problem

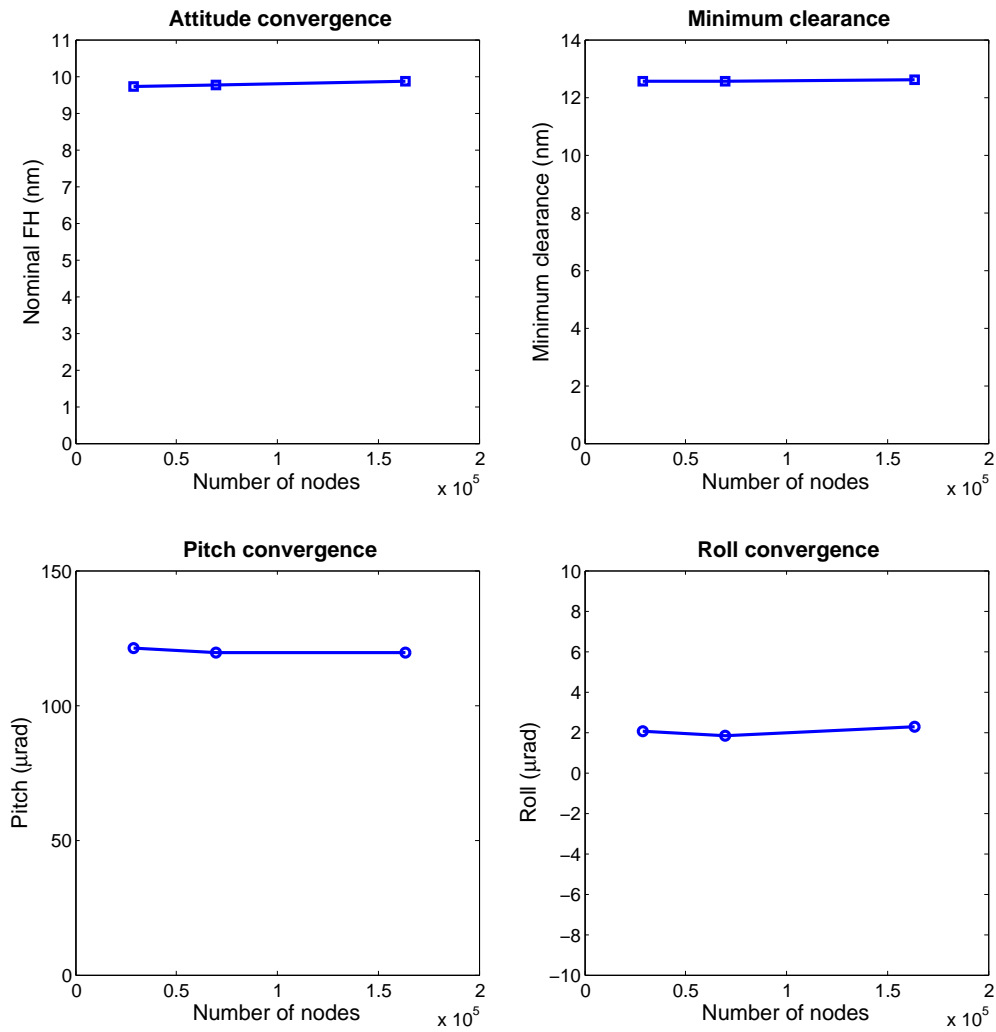Figure 10: Mesh levels for slider 1 inverse problem
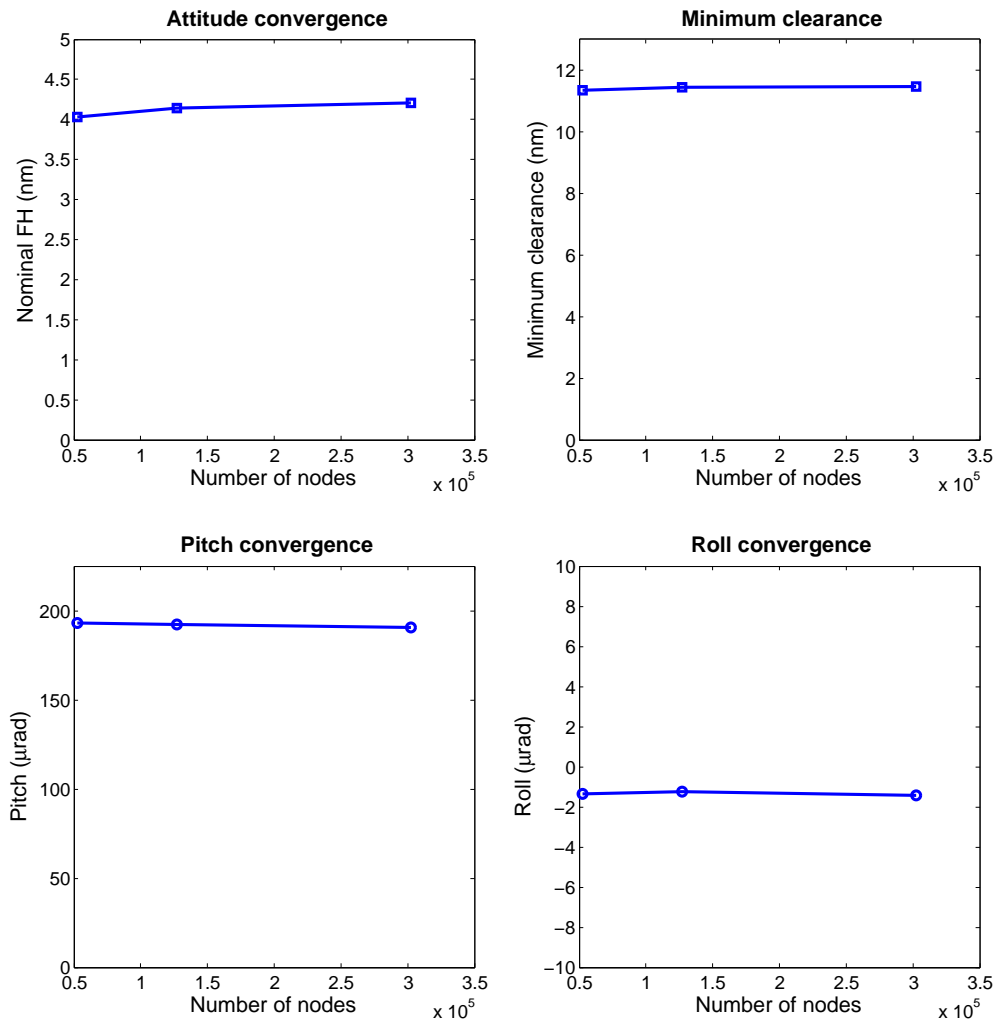
Figure 11: Grid convergence for slider 2 inverse problem

Figure 12: Grid convergence for slider 3 inverse problem